Supporting Information

Guiding Uniformly Distributed Li Ion Flux by Lithiophilic Covalent Organic Framework Interlayers for High-Performance Lithium Metal Anodes

Zihao Li,[a,b] Wenyan Ji,[b] Tian-Xiong Wang,[b,d] Yunrui Zhang,[b] Zhen Li,[b] Xuesong Ding,*[,b] Bao-Hang Han,*[,b,d] Wei Feng*[,a,c]

[a] *School of Material Science and Engineering, Tianjin University, Tianjin 300072, China*

[b] *CAS Key Laboratory of Nanosystem and Hierarchical Fabrication, CAS Center for Excellence in Nanoscience, National Center for Nanoscience and Technology, Beijing 100190, China*

[c] *Collaborative Innovation Center of Chemical Science and Engineering, Tianjin 300072, China*

[d] *University of Chinese Academy of Science, Beijing 100049, China*

Tel.: +86 022 2857 8269. E-mail: weifeng@tju.edu.cn

Tel.: +86 10 8254 5576. E-mail: hanbh@nanoctr.cn

Tel.: +86 10 8254 5708. E-mail: dingxs@nanoctr.cn

This PDF file includes:

Tables S1 to S4

Fig. S1 to S21

Table S1. The Zeta potential and average size of TpTt dispersion before and after LiTFSI addition.

TpTt Dispersion	Zeta Potential (mV)	Average Size (nm)
Before LiTFSI Addition	–34.5	774
After LiTFSI Addition	–2.1	1123

Note: LiTFSI is lithium bis(trifluoromethane)sulfonamide.

Table S2. The electrochemical parameters of symmetric batteries with and without TpTt protecting layer, and lithium transfer number calculated from potentiostatic direct current (DC) polarization and alternating current (AC) impedance spectra.

	R_0 (Ω)	R_s (Ω)	I_0 (mA)	I_s (mA)	t_{Li^+}
PP	98.88	101.78	0.0932	0.0842	0.55
TpTt@PP	65.76	62.33	0.0838	0.0748	0.84

Note: PP is polypropylene. R_0 and R_s refer to the interfacial resistance before and after AC impedance. I_0 and I_s represent the current value in initial and steady state under a polarization potential of 10 mV in DC process. t_{Li^+} is the lithium transfer number, and the value is calculated as follows.

$$t_{Li^+} = \frac{I_s(\Delta V - I_0 R_0)}{I_0(\Delta V - I_s R_s)}$$

Table S3. The comparison of the symmetric Li–Li cells for different modifications at a current density of 0.5 mA cm^{-2} and capacity of 0.5 mAh cm^{-2}.

Cycling time (h)	Voltage (mV)	Modifications	References
350	38	Magnetic field treated Li sheets	[S1]
400	30	HIO_3 chemical pretreated Li sheets	[S2]
500	100	(PVDF-HFP)/ZnO composite membrane	[S3]
900	*	Magnetron sputtering amorphous Li_3PO_4 protective layer	[S4]
1000	*	$Cu_{99}Zn$ alloy	[S5]
1000	17–31	Silicate coating Li sheets	[S6]
2450	**12**	**Lithiophilic COF interlayers**	**This work**

* The relevant result is not provided in the literature.

Table S4. The comparison of the symmetric Li–Li cells for different modifications at a current density of 1.0 mA cm^{-2} and capacity of 1.0 mAh cm^{-2}.

Cycling time (h)	Voltage (mV)	Modifications	References
300	10	Semiconductive microporous framework	[S7]
400	20	Polar PAN protecting layer	[S8]
400	20	Lignosulfonate coated separator	[S9]
400	23.3	Dual-engineered separator	[S10]
400	40	Lithium silicide protecting layer	[S11]
450	*	MgF_2/graphene framework	[S12]
500	30	Reduced graphene oxide@Li	[S13]
500	30	Nitrogen and sulfur co-doped carbon paper	[S14]
550	*	Hybrid interphase of C_{60} and Mg	[S15]
600	20	$Li_{4.4}Sn$ encapsulated in hollow graphene spheres	[S16]
744	*	Carbon fiber network	[S17]
800	54–66	Copper nitride nanowires	[S18]
850	*	Fluorinated hybrid solid electrolyte interphase	[S19]
1000	**14**	**Lithiophilic COF interlayers**	**This work**

*The relevant result is not provided in the literature.

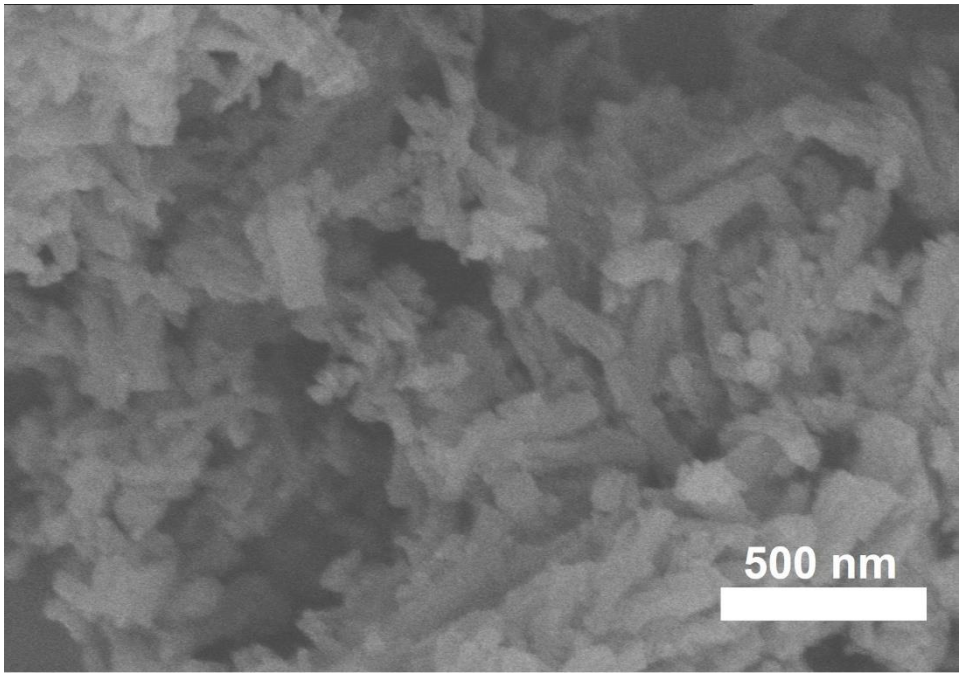

Figure S1. The scanning electron microscopy (SEM) image of TpTt.

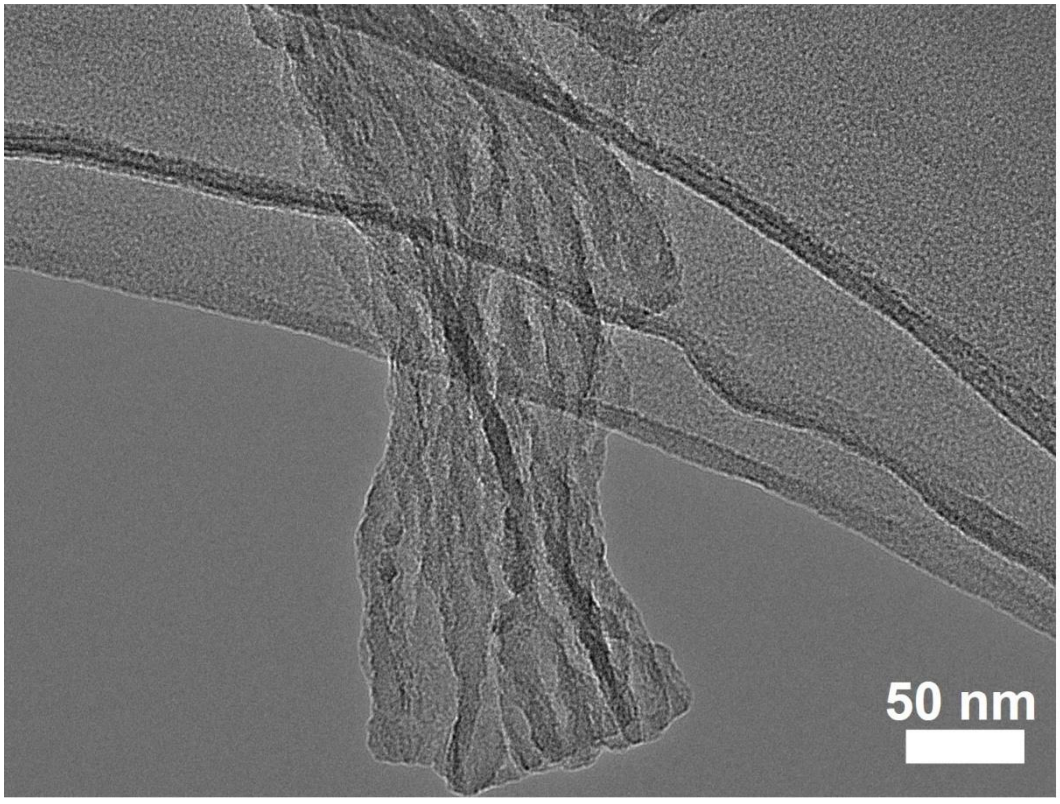

Figure S2. The transmission electron microscopy (TEM) image of TpTt.

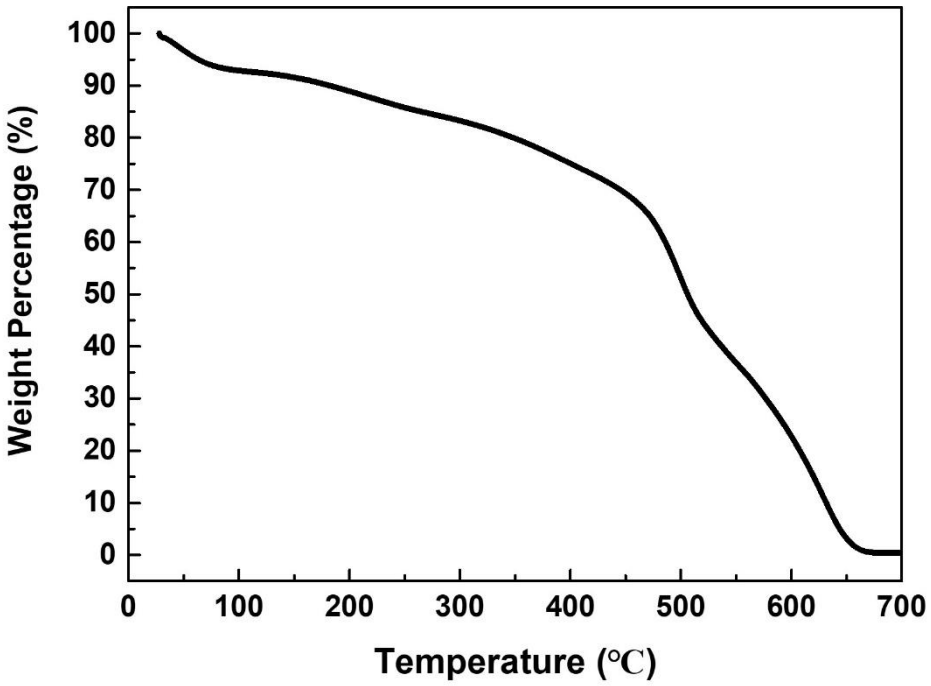

Figure S3. The thermogravimetric analysis curve of TpTt.

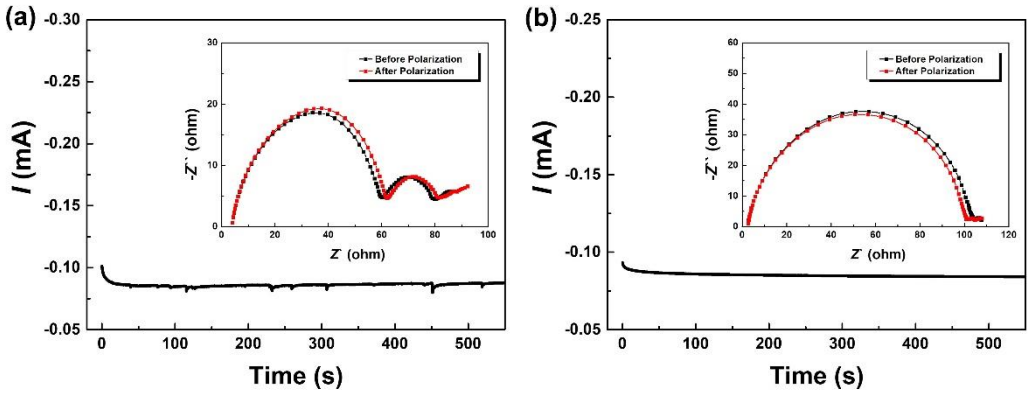

Figure S4. The potentiostatic DC polarization and AC impedance spectra of symmetric batteries (a) with and (b) without TpTt-coating separators.

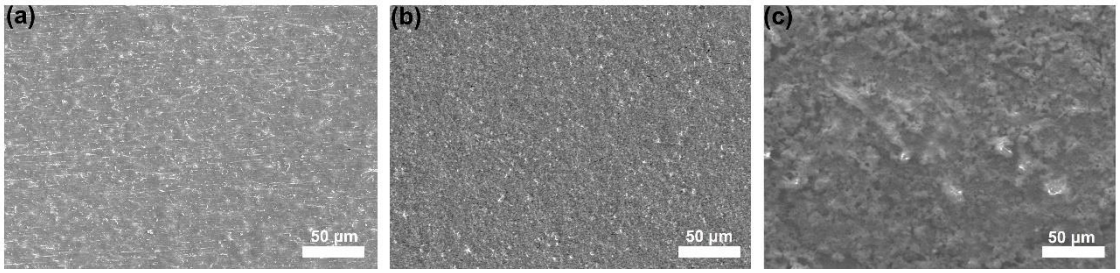

Figure S5. The SEM images of (a) pristine Cu foils, (b) TpTt and (c) Tz coated Cu foils.

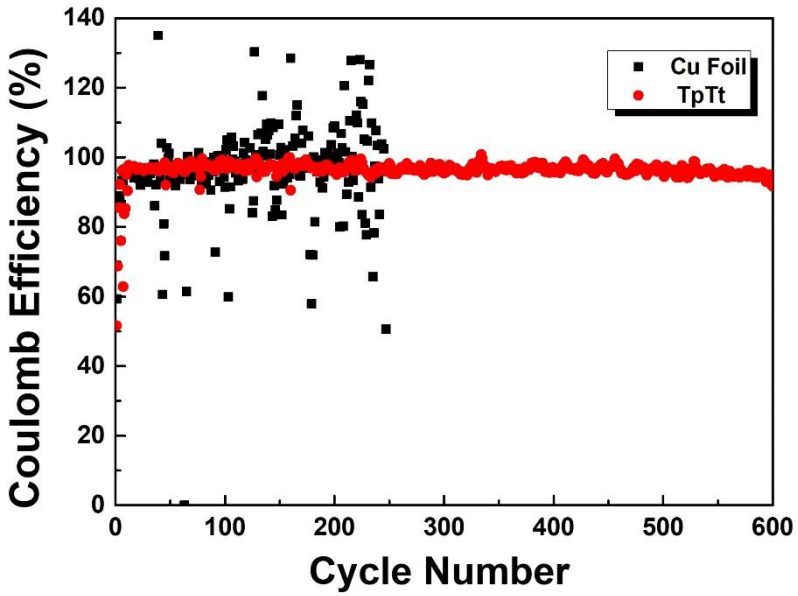

Figure S6. The Coulomb efficiency (CE) comparison of the Li–Cu batteries at a current density of 0.5 mA cm^{-2} and a capacity of 0.5 mAh cm^{-2}.

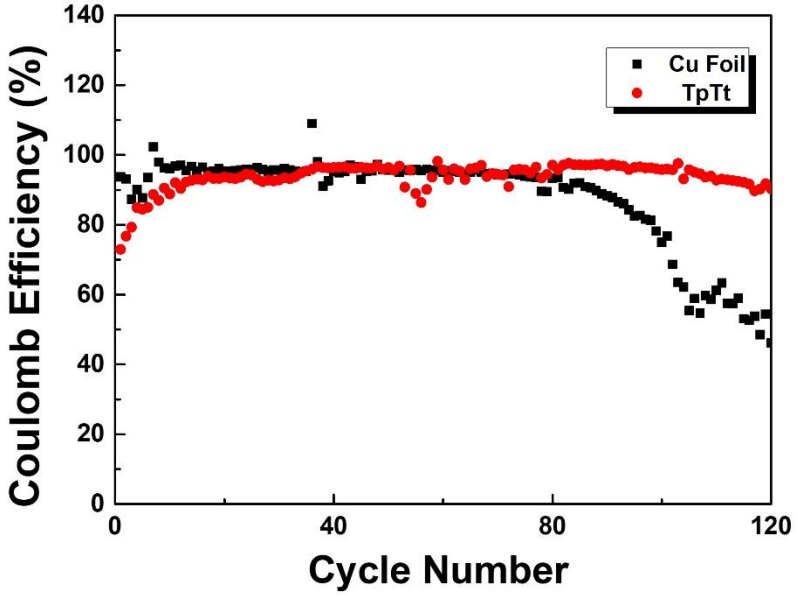

Figure S7. The CE behavior of Li–Cu batteries based on TpTt and bare current collectors at current density of 2 mA cm^{-2} with capacity of 2 mAh cm^{-2}.

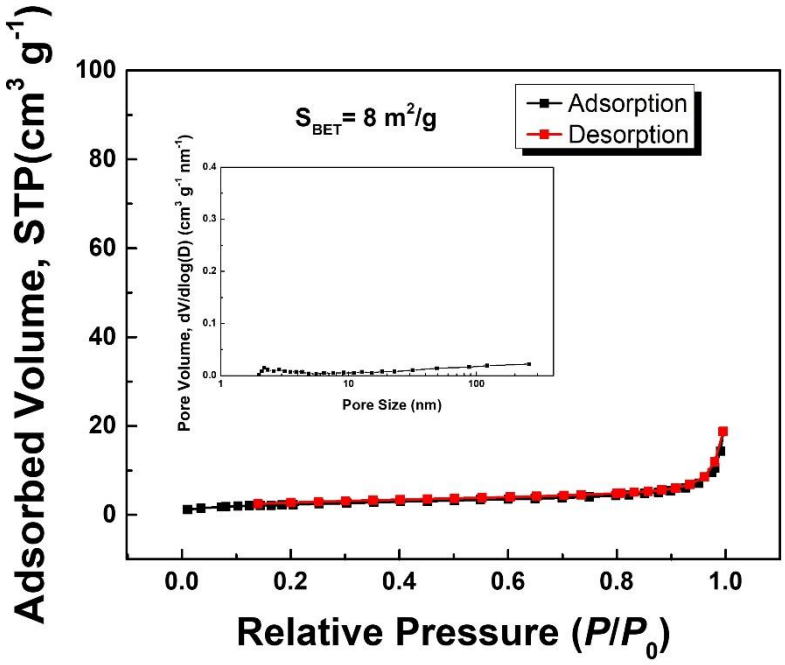

Figure S8. The N_2 sorption isotherm of Tz. The inset figure is the pore size distribution of Tz.

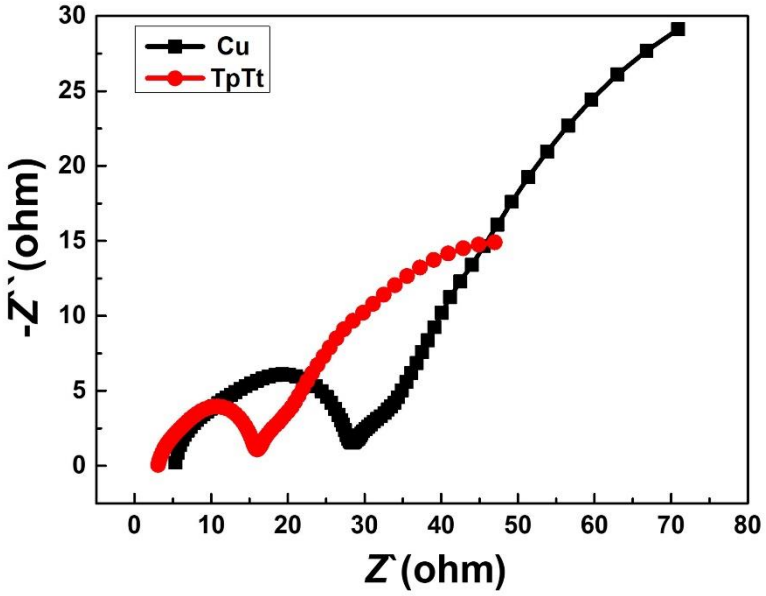

Figure S9. Comparison of Nyquist plots of the Li–Cu batteries with and without TpTt after cycling.

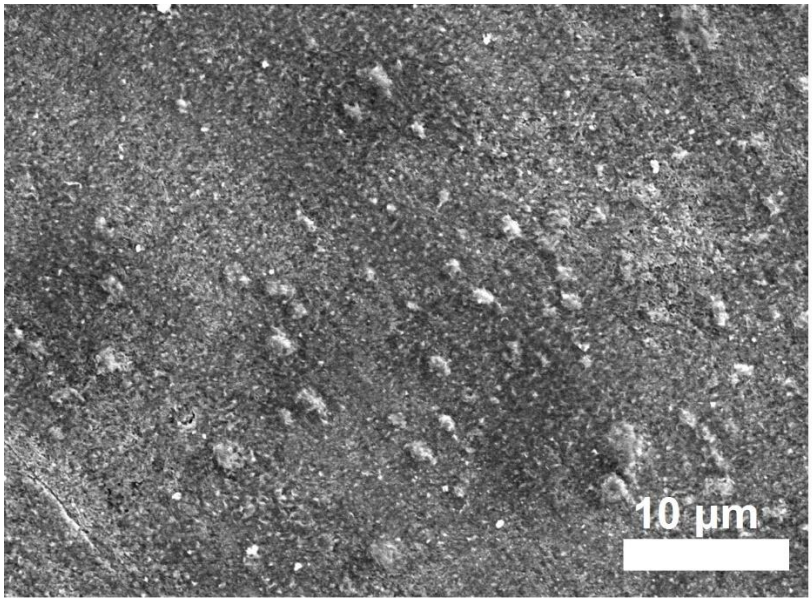

Figure S10. The SEM image of Li nucleation on Cu foils.

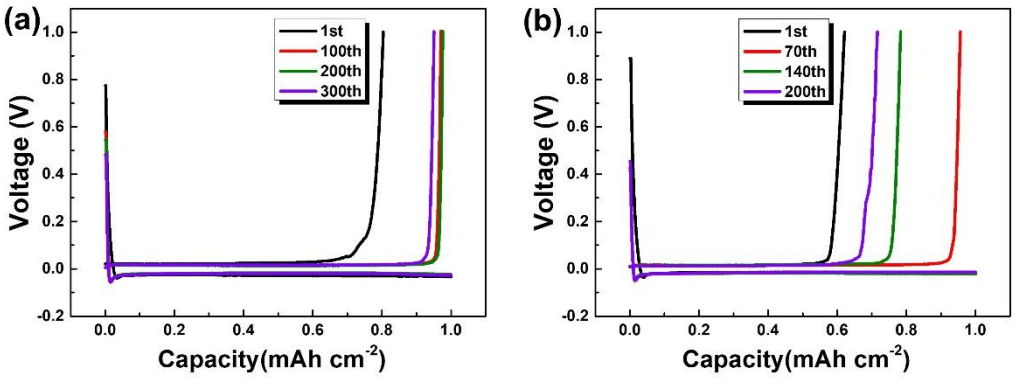

Figure S11. The voltage profiles of Li–Cu batteries based on (a) TpTt and (b) bare current collectors at current density of 1 mA cm^{-2} with capacity of 1 mAh cm^{-2} over 300 and 200 cycles respectively.

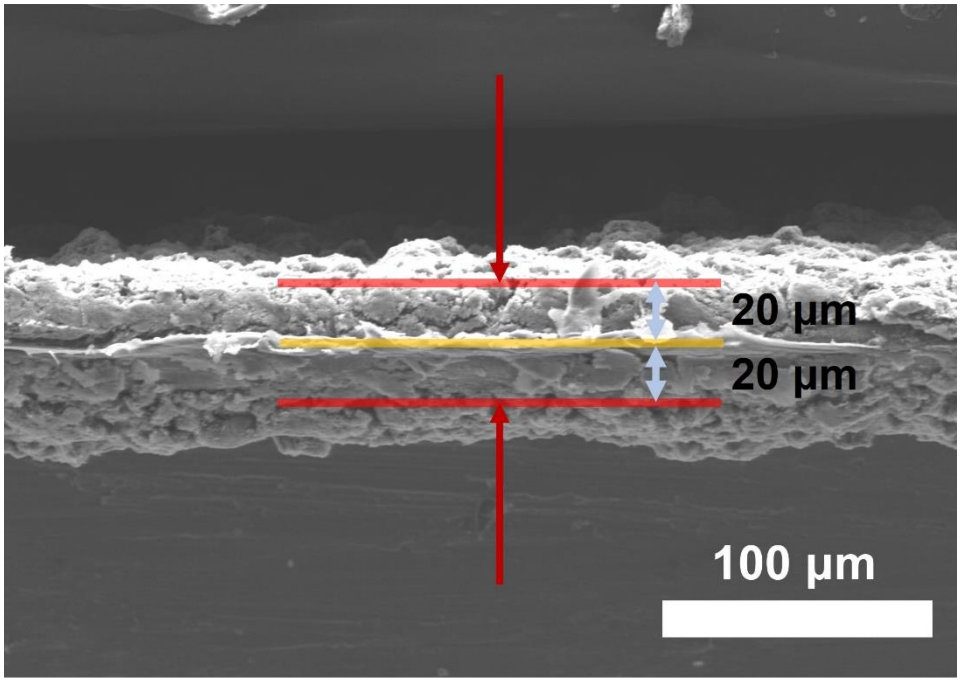

Figure S12. The SEM image of coated separators viewed in cross side.

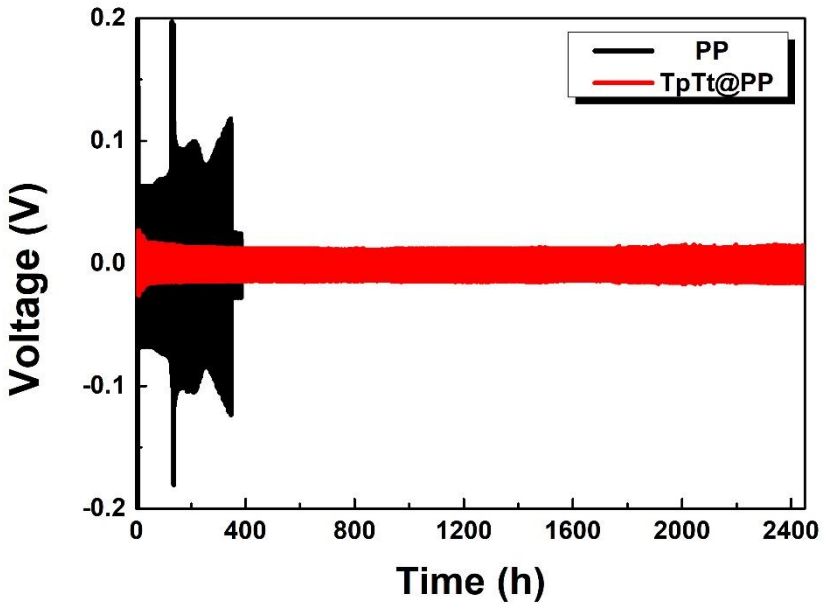

Figure S13. Comparison of the cycling stability of the symmetrical cells with and without TpTt coated separators at a current density of 0.5 mA cm^{-2}.

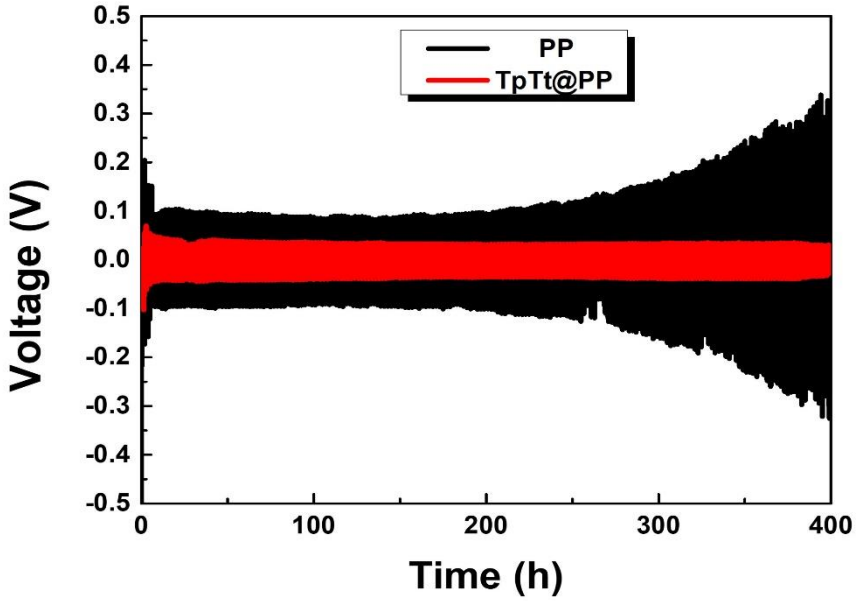

Figure S14. Comparison of the cycling stability of the symmetrical cells with and without TpTt coated separators at a current density of 2 mA cm^{-2}.

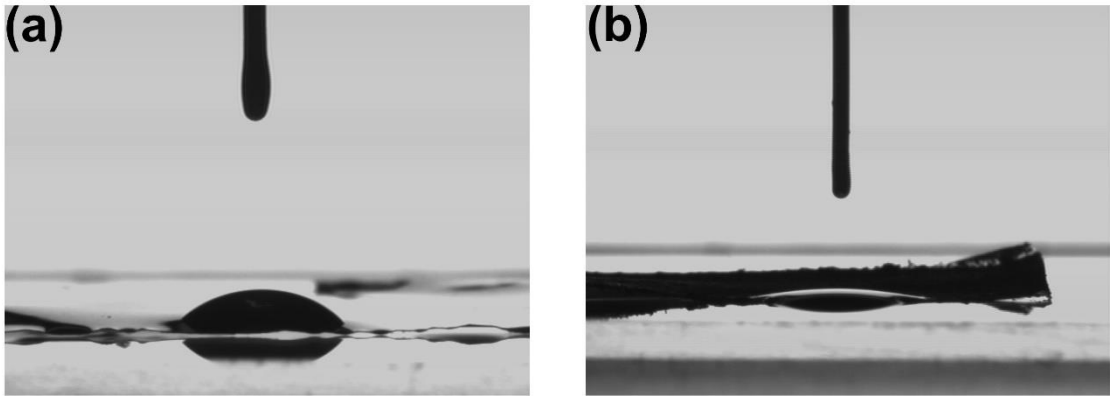

Figure S15. Comparison of the electrolyte wettability for (a) PP membrane and (b) TpTt-coated PP membrane.

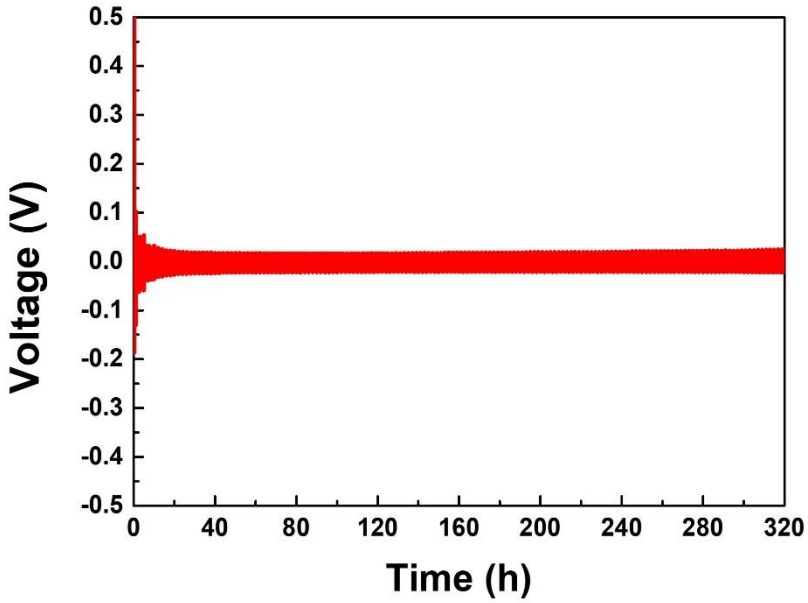

Figure S16. Cycling stability of the symmetrical Li@TpTt|Li@TpTt cell at a current density of 1 mA cm^{-2}.

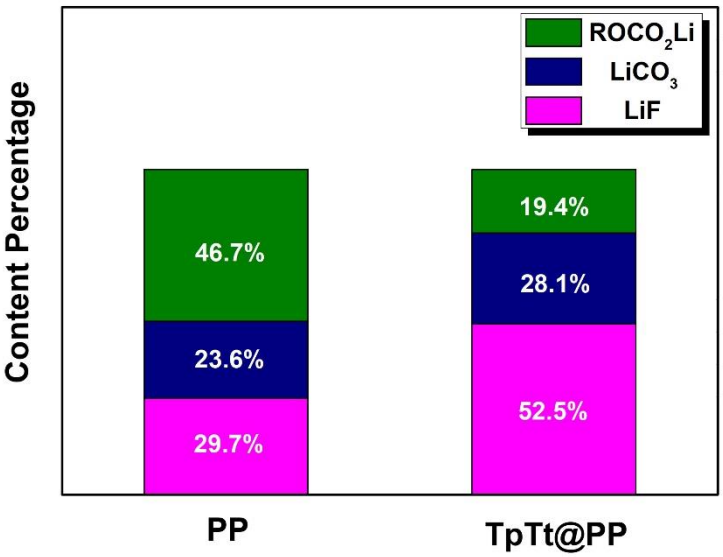

Figure S17. Comparison of solid electrolyte interphase components in half batteries with and without TpTt protecting layers after cycling.

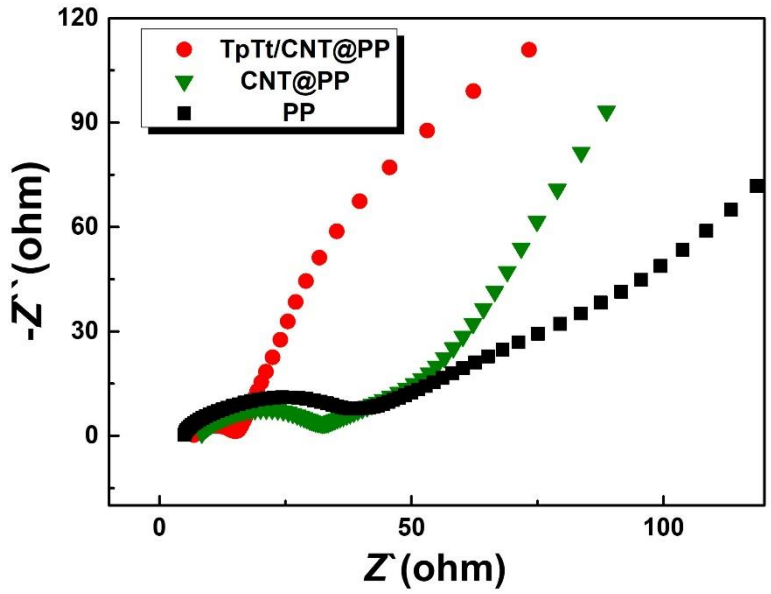

Figure S18. The Nyquist plots of Li–S batteries with TpTt/CNT@PP, CNT@PP, and PP separators after cycling.

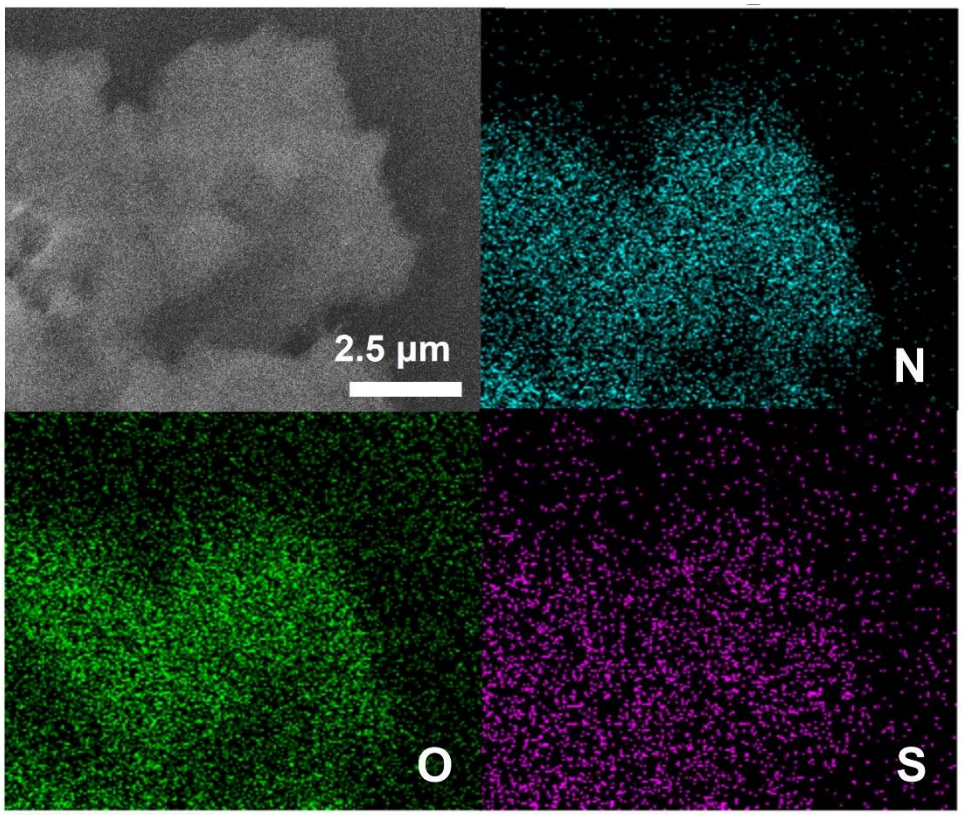

Figure S19. The elements mapping of TpTt after absorbing Li_2S_6.

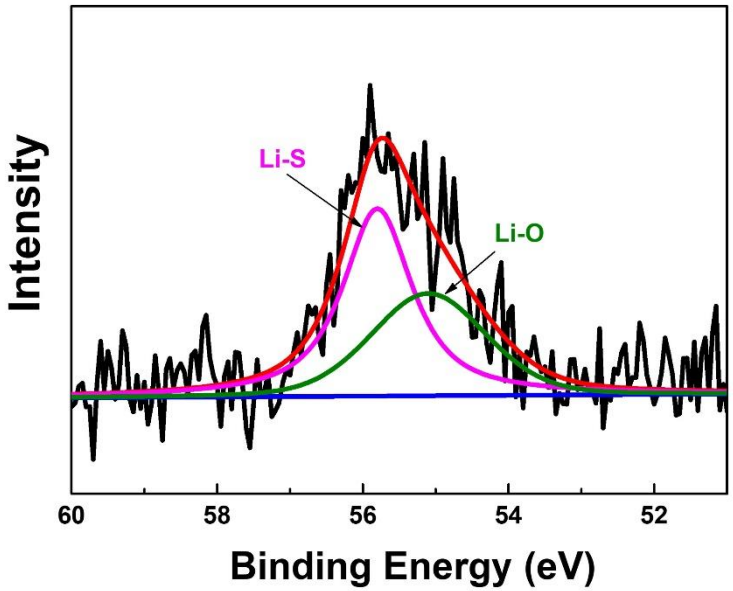

Figure S20. The Li 1s spectra of TpTt after absorbing Li_2S_6.

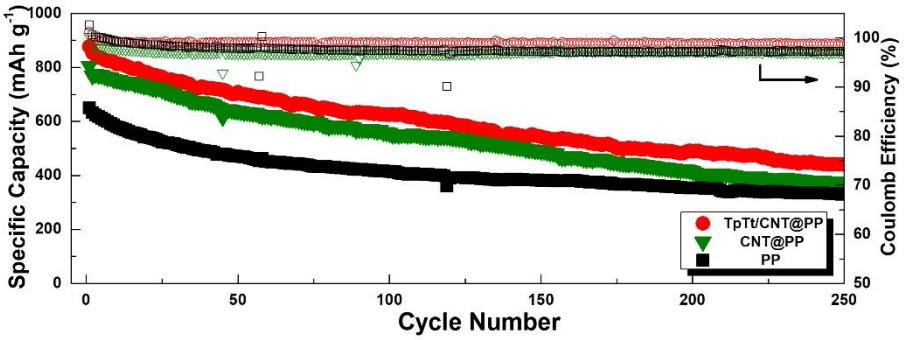

Figure S21. The long-term cycling performances of Li–S batteries with TpTt/CNT@PP, CNT@PP, and bare separators at 0.25 C.

REFERENCES

[S1] Shen, K.; Wang, Z.; Bi, X.; Ying, Y.; Zhang, D.; Jin, C.; Hou, G.; Cao, H.; Wu, L.; Zheng, G.; Tang, Y.; Tao, X.; Lu, J. Magnetic Field–Suppressed Lithium Dendrite Growth for Stable Lithium-Metal Batteries. *Adv. Energy Mater.* **2019**, *9*, 1900260.

[S2] Jia, W.; Wang, Q.; Yang, J.; Fan, C.; Wang, L.; Li, J. Pretreatment of Lithium Surface by Using Iodic Acid (HIO_3) to Improve Its Anode Performance in Lithium Batteries. *ACS Appl. Mater. Interfaces* **2017**, *9*, 7068–7074.

[S3] He, Y.; Zhang, Y.; Li, X.; Lv, Z.; Wang, X.; Liu, Z.; Huang, X. A Novel ZnO-Based Inorganic/organic Bilayer with Low Resistance for Li Metal Protection. *Energy Storage Mater.* **2018**, *14*, 392–401.

[S4] Wang, L.; Wang, Q.; Jia, W.; Chen, S.; Gao, P.; Li, J. Li Metal Coated with Amorphous Li_3PO_4 via Magnetron Sputtering for Stable and Long-Cycle Life Lithium Metal Batteries. *J. Power Sources* **2017**, *342*, 175–182.

[S5] Liu, S.; Zhang, X.; Li, R.; Gao, L.; Luo, J. Dendrite-Free Li Metal Anode by Lowering Deposition Interface Energy with $Cu_{99}Zn$ Alloy Coating. *Energy Storage Mater.* **2018**, *14*, 143–148.

[S6] Liu, F.; Xiao, Q.; Wu, H. Bin; Shen, L.; Xu, D.; Cai, M.; Lu, Y. Fabrication of Hybrid Silicate Coatings by a Simple Vapor Deposition Method for Lithium Metal Anodes. *Adv. Energy Mater.* **2018**, *8*, 1701744.

[S7] Xu, J.; Tang, W.; Yu, F.; Zhao, S.; Niu, D.; Zhang, X.; Xin, Z.; Chen, R. Trimming the π Bridge of Microporous Frameworks for Bidentate Anchoring of Polysulfides to Stabilize Lithium–Sulfur Batteries. *J. Mater. Chem. A* **2020**, *8*, 19001–19010.

[S8] Bae, J.; Qian, Y.; Li, Y.; Zhou, X.; Goodenough, J. B.; Yu, G. Polar

Polymer–Solvent Interaction Derived Favorable Interphase for Stable Lithium Metal Batteries. *Energy Environ. Sci.* **2019**, *12*, 3319–3327.

[S9] Liu, J.; Xu, R.; Yan, C.; Yuan, H.; Ding, J.-F.; Xiao, Y.; Yuan, T.-Q.; Huang, J.-Q. In Situ Regulated Solid Electrolyte Interphase via Reactive Separators for Highly Efficient Lithium Metal Batteries. *Energy Storage Mater.* **2020**, *30*, 27–33.

[S10] Ma, C.; Feng, Y.; Liu, X.; Yang, Y.; Zhou, L.; Chen, L.; Yan, C.; Wei, W. Dual-Engineered Separator for Highly Robust, All-Climate Lithium-Sulfur Batteries. *Energy Storage Mater.* **2020**, *32*, 46–54.

[S11] Tang, W.; Yin, X.; Kang, S.; Chen, Z.; Tian, B.; Teo, S. L.; Wang, X.; Chi, X.; Loh, K. P.; Lee, H.-W.; Zheng, G. W. Lithium Silicide Surface Enrichment: A Solution to Lithium Metal Battery. *Adv. Mater.* **2018**, *30*, 1801745.

[S12] Xu, Q.; Yang, X.; Rao, M.; Lin, D.; Yan, K.; Du, R. A.; Xu, J.; Zhang, Y.; Ye, D.; Yang, S.; Zhou, G.; Lu, Y.; Qiu, Y. High Energy Density Lithium Metal Batteries Enabled by a Porous graphene/MgF_2 Framework. *Energy Storage Mater.* **2020**, *26*, 73–82.

[S13] Li, N.; Zhang, K.; Xie, K.; Wei, W.; Gao, Y.; Bai, M.; Gao, Y.; Hou, Q.; Shen, C.; Xia, Z.; Wei, B. Reduced-Graphene-Oxide-Guided Directional Growth of Planar Lithium Layers. *Adv. Mater.* **2020**, *32*, 1905573.

[S14] Li, D.; Zhang, S.; Zhang, Q.; Kaghazchi, P.; Qi, H.; Liu, J.; Guo, Z.; Wang, L.; Wang, Y. Pencil-Drawing on Nitrogen and Sulfur Co-Doped Carbon Paper: An Effective and Stable Host to Pre-Store Li for High-Performance Lithium–air Batteries. *Energy Storage Mater.* **2020**, *26*, 593–603.

[S15] Xu, Q.; Lin, J.; Ye, C.; Jin, X.; Ye, D.; Lu, Y.; Zhou, G.; Qiu, Y.; Li, W. Air-Stable and Dendrite-Free Lithium Metal Anodes Enabled by a Hybrid Interphase of

C_{60} and Mg. *Adv. Energy Mater.* **2020**, *10*, 1903292.

[S16] Jiang, Y.; Jiang, J.; Wang, Z.; Han, M.; Liu, X.; Yi, J.; Zhao, B.; Sun, X.; Zhang, J. $Li_{4.4}Sn$ Encapsulated in Hollow Graphene Spheres for Stable Li Metal Anodes without Dendrite Formation for Long Cycle-Life of Lithium Batteries. *Nano Energy* **2020**, *70*, 104504.

[S17] Zhang, Y.; Wang, C.; Pastel, G.; Kuang, Y.; Xie, H.; Li, Y.; Liu, B.; Luo, W.; Chen, C.; Hu, L. 3D Wettable Framework for Dendrite-Free Alkali Metal Anodes. *Adv. Energy Mater.* **2018**, *8*, 180635.

[S18] Lee, D.; Sun, S.; Kwon, J.; Park, H.; Jang, M.; Park, E.; Son, B.; Jung, Y.; Song, T.; Paik, U. Copper Nitride Nanowires Printed Li with Stable Cycling for Li Metal Batteries in Carbonate Electrolytes. *Adv. Mater.* **2020**, *32*, 1905573.

[S19] Pathak, R.; Chen, K.; Gurung, A.; Reza, K. M.; Bahrami, B.; Pokharel, J.; Baniya, A.; He, W.; Wu, F.; Zhou, Y.; Xu, K.; Qiao, Q. Q. Dendrite-Free Lithium Deposition. *Nature Commun.* **2020**, *11*, 93.